J Solid State Electrochem (2005) 9: 698–705
DOI 10.1007/s10008-005-0646-x

ORIGINAL PAPER

S. Yu. Vassiliev · A. I. Yusipovich · Yu. E. Rogynskaya
F. Kh. Chibirova · A. M. Skundin · T. L. Kulova

Nanostructured SnO_2-TiO_2 films as related to lithium intercalation

Received: 3 August 2004 / Revised: 23 September 2004 / Accepted: 1 December 2004 / Published online: 31 March 2005

Abstract The difference in degradation behavior of titania-doped tin dioxide films is explained by a pronounced effect of the doping level on the film dispersity and fine distribution of titania. A two to three times decrease in nanoparticles sizes in the doped films compared with nanoparticles in SnO_2 film (20–30 nm) is revealed by using scanning tunneling microscopy (STM). Such STM data (measured in ex situ configuration) combined with XRD and Mössbauer spectroscopy analysis confirm that the nanoparticles are composed of nanostructured heavily disordered SnO_2 and TiO_2 rutile solid solution or of amorphous phase containing both SnO_2 and TiO_2, the content of the crystalline and amorphous phases being approximately equal.

Keywords Tin dioxide · Lithium intercalation · Scanning tunneling microscopy and spectroscopy · Nanostructure

Introduction

Nanostructured SnO_2-based compositions well-known as materials for gas sensors [1, 2] were recently found to be also prospective candidates for lithium batteries [3–5]. The initial cathodic polarization of doped tin oxides in solutions of lithium salts results in the irreversible reduction of oxide with formation of metallic tin. Thus formed metallic tin dispersed in oxide matrix demonstrates the reversible absorption–desorption of lithium with formation of intermetallic compound $Li_{4.4}Sn$. Correspondingly, irreversible (observed in the course of initial charging) and reversible contributions to capacity can be separated. The size of initial oxide particles is responsible for the values of capacity components and stability of lithium recharging (see, for example, in Ref. [4]). A serious problem results from the gradual increase in the size of metal particles, which, in turn, induces the decrease in reversible capacity with respect to lithium.

An alternative concept of lithium intercalation by tin oxides stresses the role of Sn–O–Li nanoscale phases, not intermetallic compounds. The stability of nanoscale phases in relation to reduction by lithium determines slower growth of tin crystallites [6]. When some foreign oxides (such as B_2O_3, Al_2O_3, or P_2O_5) are inserted to form dispersed amorphous tin-based composite oxides, the best long-term cycling is achieved as a result of high stability with respect to reduction [7].

Nanoheterogeneous titania-doped tin oxide films prepared by thermohydrolytic decomposition of $SnCl_2$ and $TiCl_4$ solutions can be considered as prospective charge-accumulating materials because of high conductivity, nano-scale size of constituents, and mechanical stability in the course of prolonged cycling in aqueous solutions [1, 2]. For lithium accumulation by the films of this type [8, 9], the reversible capacity up to 650 mA h g^{-1} is found, with satisfactory cycling stability.

Structural studies of multicomponent oxide film electrodes (electrocatalysts, etc) prepared by the above-mentioned technique show that the reaction of hydrated species in solution followed by heat treatment results in the formation of unusual nonequilibrium phases—nanoheterogeneous solid solutions [10, 11]. They have been found to be a mixture of various oxide nanoclusters (RuO_2, TiO_2, IrO_2, SnO_2) of less than 1–2 nm size, which are statistically distributed in amorphous matrix formed by their hydrated precursors.

S. Y. Vassiliev (✉) · A. I. Yusipovich
Department of Electrochemistry, Faculty of Chemistry,
Moscow State University, Moscow, Russia
E-mail: wasq@elch.chem.msu.ru

Y. E. Rogynskaya · F. K. Chibirova
Research centre "Karpov Institute of Physical Chemistry",
Moscow, Russia

A. M. Skundin · T. L. Kulova
Frumkin Institute of Electrochemistry
Russian Academy of Sciences,
Moscow, Russia

According to STM, XRD, and XPS studies, SnO_2 films containing 10 mol % TiO_2 (ST10), annealed at 450 °C consist of globules of 15–20 nm size, which in turn have a fine nanostructure [1, 2, 11]. The cores of these globules contain crystallites of (Sn, Ti)O_2 rutile solid solution (6–8 nm) pierced with amorphous SnO_2 strips. Similar amorphous SnO_2 layers containing up to 15% SnO cover the globule surface. Such a nanostructure in ST10 films is due to the formation of the crystalline $SnCl_2$ intercalation phase as their precursor, which contains inclusions of polynuclear titanium–tin oxohydroxo complexes.

Some two to three times larger titania-free SnO_2 globules were observed [11]. Hydrous tin oxide, which was formed in the course of condensation of polynuclear species $[SnO_x(OH)_y]_n$ has been found [11] to be the precursor of that phase. The latter species result from hydrolysis of $[Sn(IV)Cl_4]L_2$ (L = OH, H_2O) complexes presenting in initial $SnCl_2$ solution due to the partial oxidation Sn(II) - > Sn(IV).The role of TiO_2 in creating high charge-storing properties of SnO_2 remains unclear.

The aim of this work was to obtain single-phase SnO_2-based materials with a variable TiO_2 content and to study their structure, morphology, and electrochemical properties. At this stage, the study is limited to freshly prepared films, providing the basis for further understanding of microstructure and nanostructural changes induced by lithiation/delithiation. In this study, we report as observed by using of STM, X-ray diffraction, and Mössbauer spectroscopy.

Materials and methods

The condition of the synthesis of a new series of SnO_2 – TiO_2 films (further designated as ST x, where $x = 0$, 10, and 20 mol % TiO_2[1]) are described. While the concentration of $SnCl_2$ solution remained the same as in [1, 2, 8] (0.067 M), the concentration of $TiCl_4$ was increased by order of magnitude and amounted to 1 M. It is known that in aqueous hydrochloric acid solution of $TiCl_4$ ($c_{Ti} = 0.01$–0.05 mol/l and $c_{HCl} = 0.1$–2.0 mol/l) mononuclear and polynuclear forms of Ti (IV) hydroxyoxo complexes existing for the latter $[(TiO)_8(OH)_{12}]^{4+}$ species predominate [12]. The increase in $TiCl_4$ concentration (0.35–1.2 mol/l) ($c_{HCl} = 1$ mol/l) resulted in the increase of the number of polynuclear complexes and the degree of their polymerization. These polymeric species appear in essence to be the nuclei of the hydrated titanium oxide [13]. The solutions were applied layer by layer on to titanium supports pretreated by mechanical polishing and etching in sulfuric acid. The temperature of annealing was 450°C for doped films, and 350 and 450°C for pure tin oxide.

[1]The fabrication mode differed from that previously used in [1, 2, 8], so the samples denoted ST10 and ST20 are not identical to the samples described in these references.

X-ray dispersion analysis confirmed that the content of SnO_2 and TiO_2 in films matched the nominal composition of Sn and Ti cations in original solution. Besides, about 1% of chlorine was found. The XPES analysis showed that about 25% of oxygen atoms were present in hydroxogroups and 5% in aqua groups.

For electrochemical measurements, 1 M $LiN(CF_3SO_2)_2$ in dioxolane was used as electrolyte (water content below 70 ppm). Compartments of the three-electrode cell were separated with porous membranes (polypropylene PORP). Potentials were measured and are referred below in comparision with lithium reference electrode. Before starting the experiments, oxide films were additionally dried under vacuum at 120°C for 8 h. EL-2 potentiostat designed in the Frumkin Institute, RAS, was used.

For XRD, DRON-3 M diffractometer run by PC was used. For the decomposition of intensity profiles to multicomponent spectra PROFITVZ program [14] was used. We could not perform a quantitative analysis for the electrodes studied, since the lines of titanium support superimposed practically all intensive rutile lines (besides 110) and prevented correct decomposition of mixed maxima. The instrumental broadening b was too small (0.21 degree 2θ) to make the corrections in FWHM (full width at half maximum) value, therefore the latter was considered as β (diffraction broadening).

The samples were studied with a conventional Mössbauer spectrometer. The velocity drive of this spectrometer operates under the constant acceleration mode over 1024 channels. The velocity scale of the Mössbauer spectra was calibrated with a reference spectrum of metallic iron. All measurements were carried out at room temperature. The conversion electron Mössbauer spectroscopy (CEMS) measurements were carried out using a gas detector with He + 5% CH_4 as the flow gas. In the (CEMS) method, internal conversion electrons and Auger electrons associated with the deexcitation of Mössbauer nuclei are detected in the sample under study. Due to the short range of electrons in solids this method is especially convenient for studying subsurface regions of the order of a few hundreds atomic layers. 5 mCi $CaSn^{119m}O_3$ was used as gamma-ray source in this experiment.

For tunneling microscopy experiments, homemade LitScan-2 device with extended spectroscopic facilities was used. Pt–Ir tips (10% Ir) of 0.5 mm diameter were mechanically sharpened. In topographic experiments, bias was 1.3 V (positively polarized tip), and STM current was 0.3 nA. The technique of measuring the local spectra is discussed in detail in [15]. Voltage–current spectra were measured under a pulse mode, in order to avoid the shift of tip location in the course of measurements. Voltage–distance spectra were registered under an open feedback loop, with the scan rates not exceeding 0.5 V s^{-1}. Numerous (100–150) repeated measurements of current–voltage and voltage–distance spectra were carried out for all samples. These data were collected for various points inside the area within the

limits of piezo-manipulator movement, and also for various surface regions and experimental sets. Good reproducibility of the key characteristic features of the tunneling spectra was found for each certain type of oxide. Most typical spectra without any averaging or pretreatment are presented in this article.

Results and discussion

X-ray analysis revealed that ST10 and ST20 films were contained a single crystalline phase. The decomposition of the profile of each reflection by program PROFITVZ evidenced that only one rutile phase gave the contribution to the intensity profile. Maxima in the mixed film patterns are very weak and diffuse (Fig.1).

That effect may point to the dispersion of crystallites or/and to the microdistortions (disordered crystal structure), as well as to the presence of amorphous phase. The crystallinity of the SnO_2 electrode is much higher. The increase of reflection FWHM with the 2θ (Bragg angle) proportional to tg θ [16] testifies to the existence of microdistortion in ST10 and ST20 electrodes. This may be connected with disordered structure of the mixed phase containing SnO_2 and TiO_2. This fact does not allow a correct estimation of crystal size from the XRD data. The FWHM of the SnO_2 film (amounting to 0.854) practically does not change with 2θ, which points to the effect of crystallites dispersion as the main contribution in the width of lines. In the latter case the average size of crystallites, of about 11 nm, was calculated by means of Sherrer formula [16].

The integral intensities of (110) reflections were 148, 80, and 80 relative units for the films with $x = 0$, 10, and 20, respectively; however, the heating of plain SnO_2 film up to 450°C resulted in the increase of line intensity of main strong lines [$\sim$ 20% for (110), and 40% for (101) and (301)], that is, the degree of crystallinity increased. All these data permit us to estimate that the content of amorphous phase in mixed films is higher than 50%.

The rutile cell parameters a and c for all three samples are given in Table 1. The remarkable decrease of a and c in titania-containing films in comparison with undoped one means that some type of solid solution has been formed. The decrease of rutile lattice periods from the values typical for tin oxide my be explained by the lower ion radius of Ti^{4+} (0.064 nm) in comparison to the radius of Sn^{4+} (0.071 nm)

Refinement of film morphology and determination of the Sn atoms oxidation state and their local surrounding have been solved by using of ^{119}Sn MS. The analysis of Mössbauer spectra [the main characteristics of the MS such as chemical shift (δ), quadrupole splitting (E), and relative intensity, A (area of spectra) are given in Table 1] leads to the following conclusions.

1. According to the magnitude of relative absorption ($\sim$60%), the spectrum of the SnO_2 film (Fig. 2) corresponds to a solid sample with a high degree of crystallinity, while the spectra of the films with $x = 10$

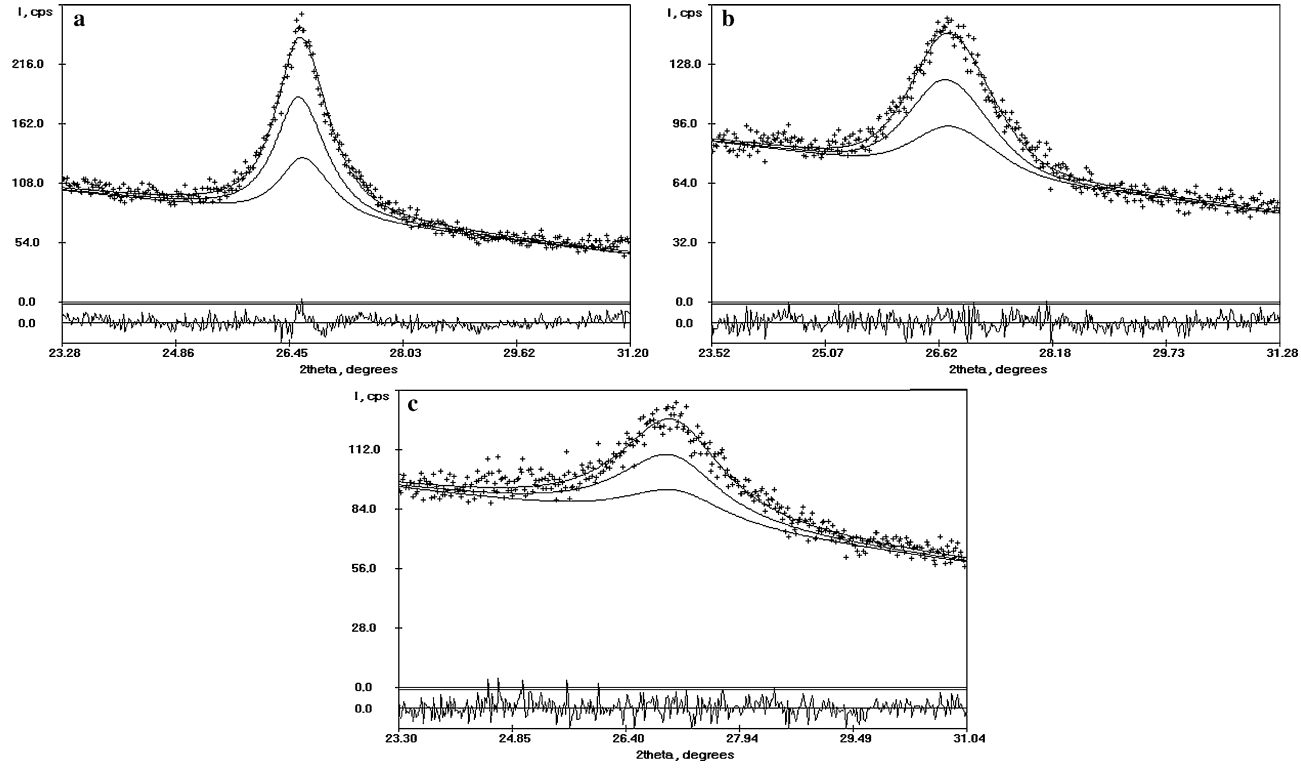

Fig. 1 The results of the decomposition of (110) reflection to possible multicomponents. *a*, *b*, and *c* present the decomposition of (110) reflection for SnO_2, ST10 and ST20 electrodes, respectively, and show doublet (α_1 and α_2) for only one rutile phase

Table 1 XRD and Mössbauer spectra data for SnO_2 – TiO_2 films

Electrodes ST x	Rutile cell periods (nm)	D^a_{av}(nm)	Mössbauer spectra data			
			Tin oxide doublet	δ, (mm/s) vs. $CaSnO_3$	ΔE,(mm/s)	A,(%)
SnO_2(x = 0)	a = 0.4734 c = 0.3175	11.0 ± 1.0	SnO_2	–0.0076 ± 0.0016	0.532 ± 0.004	98.34
			SnO	2.83 ± 0.12	1.91 ± 0.12	1.72
ST10 (x = 10%)	a = 0.4705 c = 0.3165		SnO_2	0.0122 ± 0.0038	0.511 ± 0.010	93.45
			SnO	2.951 ± 0.072	1.82 ± 0.13	6.55
ST20 (x = 20%)	a = 0.4670 c = 0.3118		SnO_2	0.0176 ± 0.0043	0.516 ± 0.012	98.05
			SnO	2.85 ± 0.12	2.08 ± 0.24	1.95

[a] The average size of crystallites determined with the use of FWHM for (110) reflection by Sherrer method. ($D_{av=0.94\lambda/\beta\cdot\cos\theta}$, $\lambda_{Cu-K_{z_1}}$ = 0.1541 nm [16])

and 20 can be attributed to solids with a high degree of amorphous SnO_2 due to remarkably lower relative absorption.

2. A doublet typical of the Sn atoms in SnO_2 represents the main contribution in all three films (93–98%); some increase in the chemical shift, δ, in the spectra of mixed films in comparison to the SnO_2 film may be associated with a small lengthening of the Sn – O bonds in amorphous SnO_2 due to the change in the s – p bonding.
3. The distinctly remarkable second doublet observed for all spectra is attributed to the partly hydrated SnO that is localized at the surface. Detailed studies by XPS and inverse photoemission spectra [18, 19] demonstrated that these "SnO" states are present on the disordered surface of SnO_2 or in nanosized SnO_2 crystallites. Disorder of SnO_2 results in the loss of the symmetry center of the Sn^{4+} cation octahedral surrounding, in the splitting of Sn5s and Sn5p atomic orbitals and emerging of hybrid 5s–5p orbitals, which are displayed as Sn^{2+} states. So "SnO" surface states are indicative of tin atoms in SnO_2 disordered grain boundaries. The non-monotonous dependence of Sn^{2+} content on titania content will be discussed below. Analysing the XRD and MS results together, one can notice two contradictory phenomena: in spite of the remarkable change of rutile cell periods in the films studied, only a small increase in chemical shift (δ) with TiO_2 content is observed.

This contradiction is removed if one were to take into consideration the fact that the amorphous SnO_2 dominates in mixed films while the crystalline rutile phase appears in less quantity, as evidenced by XRD. In such a case, the amorphous SnO_2 gives a higher contribution to the Mössbauer parameters of mixed films than does the tin oxide involved into rutile solid solution. The higher degree of amorphous state in mixed films compared to SnO_2 film results in the small lengthening of the Sn–O bonds; however this effect is not related to crystalline SnO_2 in solid solutions, that is the influence of titanium oxide on electronic parameters of crystalline SnO_2 was not revealed.

The electrochemical behavior of the one films under study was similar to the one previously observed for titania-doped tin oxide films described in [8, 9]. Galvanostatic charge–discharge curves (first cycle) of the samples with various titania content demonstrate no pronounced difference of capacities, whereas the irreversible capacity is noticeably higher for ST20 sample (Fig. 3). For pure tin oxide (curve 1, Fig. 3) a plateau at c. 1 V is observed, which corresponds to reduction with formation of tin metal; parallel formation of lower valency oxides also cannot be excluded in this potential region [8]. For titania-containing films, a similar reduction process takes place in a wider potential region and

Fig. 2 Mössbauer spectra of SnO_2–TiO_2 films. **a** – SnO_2, **b** – ST10

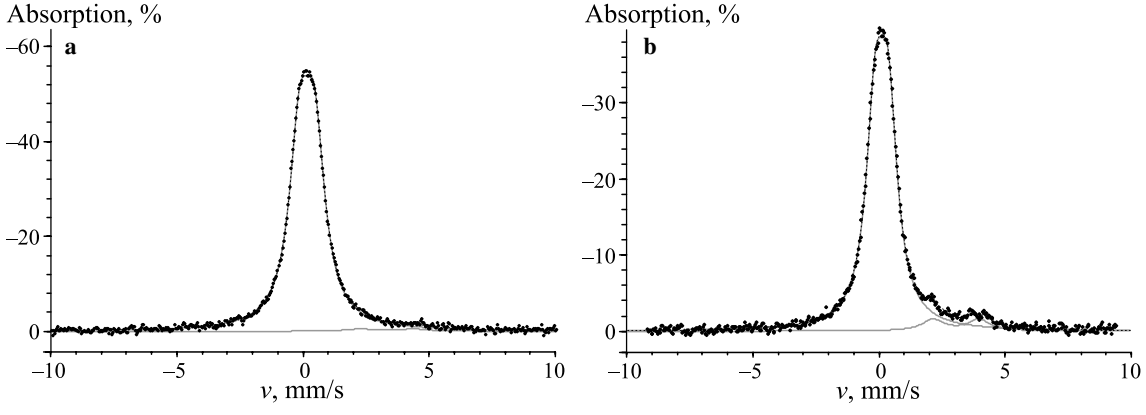

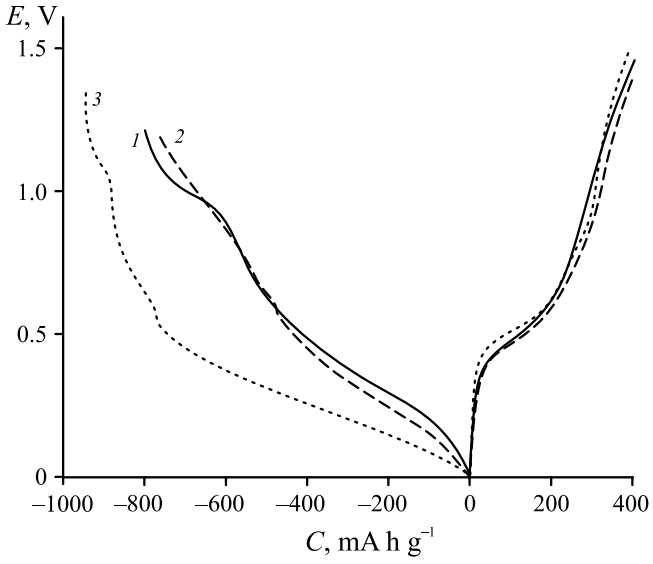

Fig. 3 Charging curves of tin dioxide films (first cycle) measured in 1 M $LiN(CF_3SO_2)_2$ in dioxolane. *1* SnO_2, *2* ST10, *3* ST20. Current density 80 mA g^{-1}

does not demonstrate any special electrochemical features. This behavior can be explained both by kinetic reasons and more the pronounced heterogeneity of doped samples. The role of dispersion cannot be clarified at this stage.

Despite close reversible capacities observed for the first cycle, the decrease of capacity in the course of subsequent cycling depends on the titania content (Fig. 4). We now concentrate on understanding the micro(nano)structural doping effects which induce such an essential difference in degradation behavior.

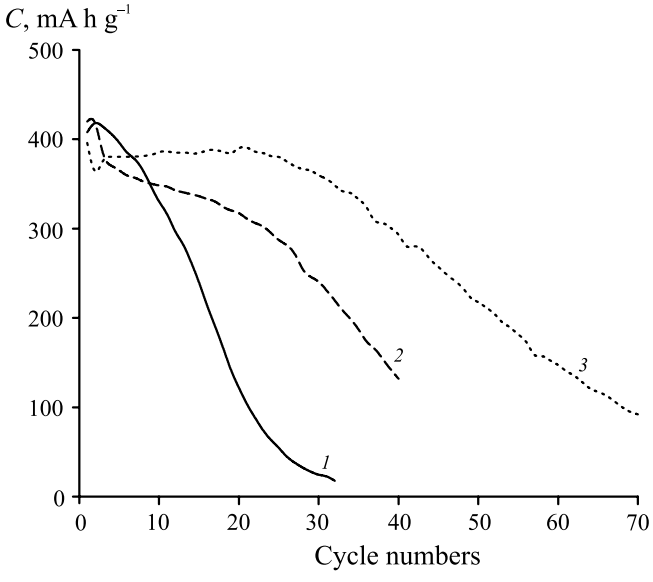

Fig. 4 Cyclic stability of the reversible capacitance. *1* SnO_2, *2* ST10, *3* ST20. Current density 80 mA g^{-1}

Figures 5b-d present typical STM images of the films in a micrometer scale. An image of the titanium support is given in Fig. 5a for comparison. It is easy to see deep scratches formed in the course of mechanical polishing. Fast oxidation of titanium surface induced by the tip is accompanied by formation of loose, poorly conducting oxide. The films under study demonstrate another type of topography, consisting of smooth globules 200–700 nm in size. The globules consist of smaller nanoparticles, whose size decreases sharply with the increase of titania content (Fig. 6). Crystal size estimated from STM data for SnO_2 film, taking into account image distortions induced by tip non-ideality [17]) are found to be in agreement with the sizes estimated from XRD data (Table1). These data indicate the higher dispersion of titania-doped films. The clarity of STM images decreases in the sequence ST0–ST10–ST20, as it can be seen in Fig. 6. Loss of clarity can result from the increase in the content of amorphous phase.

Tunneling spectra (Fig. 7) demonstrate the decrease of films conductivity with titania content, and also the more pronounced resistive heterogeneity for higher doping levels. The low conductivity of ST20 films makes it difficult to fix an STM tip and decreases the quality of STM images of these films. One–two orders of increase in the resistance of STM gap at positive currents (i.e. for the highest contributions of film resistance) is found.

Separation of the contribution of the air gap and film resistance to the total STM gap resistance presents a special problem. With increase of film resistance, the effect of the film on the slope of voltage–current spectra rises sharply. The reason is as follows: at certain fixed base values of bias and current under equilibrium conditions the resistance of the air gap for more resistive films should be much lower, in order to compensate for the increased contribution from the film. Correspondingly, we can conclude that there would be a several-order increase in the specific resistance of the films with titania content. Direct conductivity measurements are complicated by low film thickness and the existence of a more conducting support.

Qualitatively, the observed resistance–composition dependence agrees well with previous data of direct conductivity measurements of similar films on insulating supports [2].

The increased heterogeneity of local conductivity, observed for the films with higher titania content can be referred to more pronounced heterogeneity of chemical/phase composition. For ST20, the heterogeneity results in a one-order difference of the slopes of voltage–current spectra measured in various points (curves 3 and 4 in Fig. 7). For less-doped films, difference in local conductivity of various areas is clearly seen in more sensitive voltage–distance spectra (Fig. 8). For certain points, these spectra are smooth, with the changes of distance below 5 nm (curve 1 in Fig. 8). Curves of this type correspond to more conductive areas. Spectra of similar shapes with close distance values were obtained for pure tin dioxide also. For some other areas (whose topo-

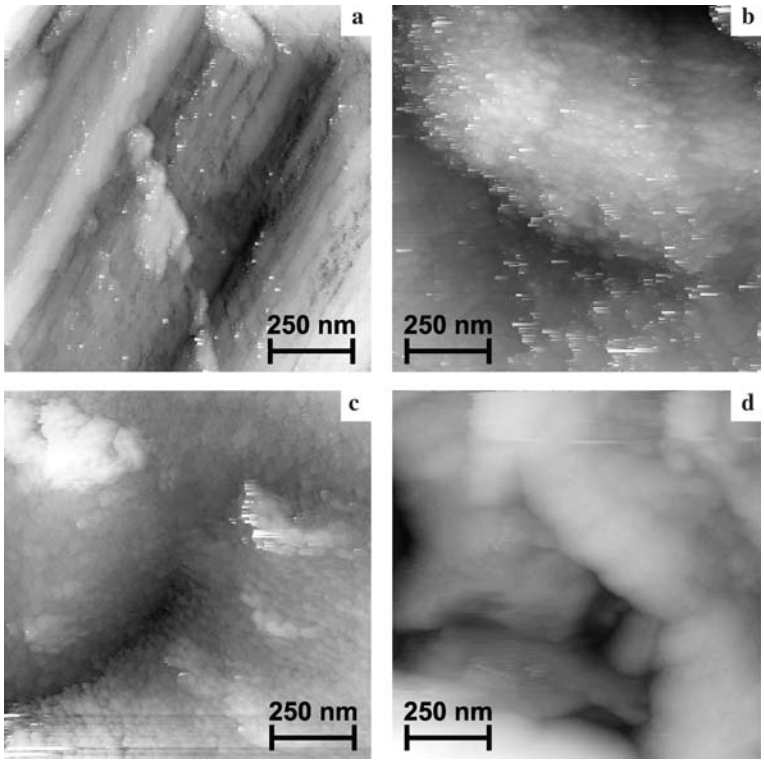

Fig. 5 Micrometer scale STM images of titanium support (**a**) and tin oxide films. **b** SnO_2, **c** ST10, **d** ST20

graphic images usually look more cloudy) the voltage–distance spectra are asymmetric and include stepwise features with distance changes of 50–100 nm (curve 3 in Fig. 8). We associate this sharp distance increase with the fact that at low voltages the film conductivity is too low for passing the established current. Under the constant current mode, this situation results in closer approaching of tip and appearance of direct tip–sample contact, with partial penetration of tip into the film. In the framework of this hypothesis, the appearance of

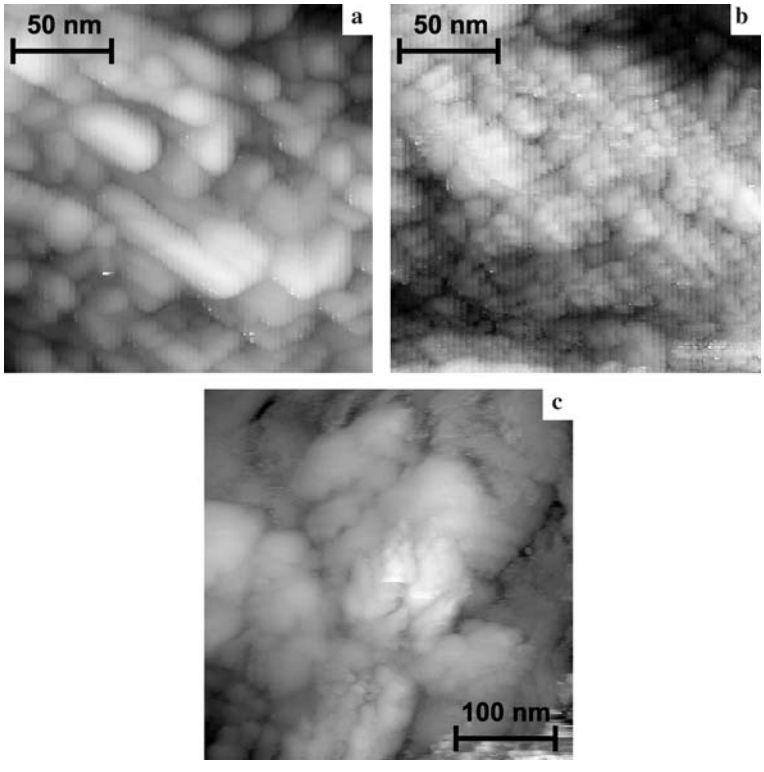

Fig. 6 Nanometer-scale STM images of tin oxide films. **a** SnO_2, **b** ST10, **c** ST20

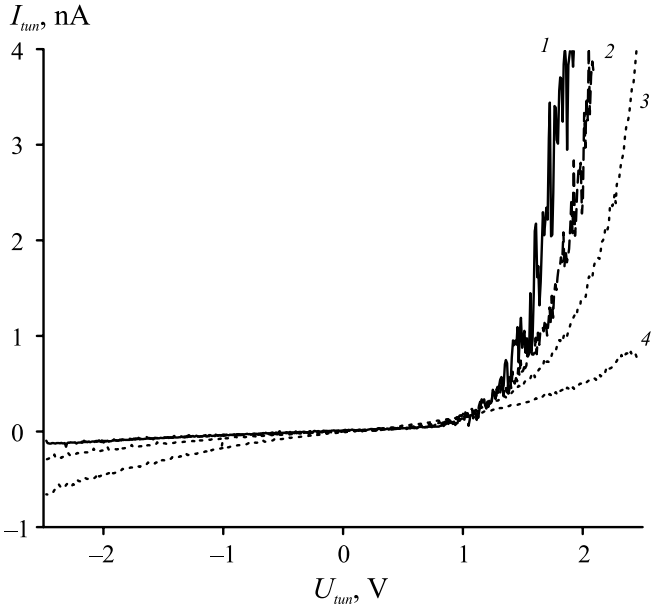

Fig. 7 Local voltage–current spectra obtained for tin dioxide films. *1* SnO_2, *2* ST10, *3,4* ST20. (curves typical of various points of heterogeneous sample)

stepwise features manifests a much higher local resistance of the areas under study.

There are many surface areas for which an intermediate type of voltage–distance spectral behavior is observed (curve 2 in Fig. 8), and, correspondingly, intermediate values of conductivity can be concluded for these areas.

For ST20 samples, stepwise behavior of voltage–distance spectra is observed for any point of the surface. Typical distances appear to be up to 1 μm, which exceeds the vertical resolution of the STM device. This

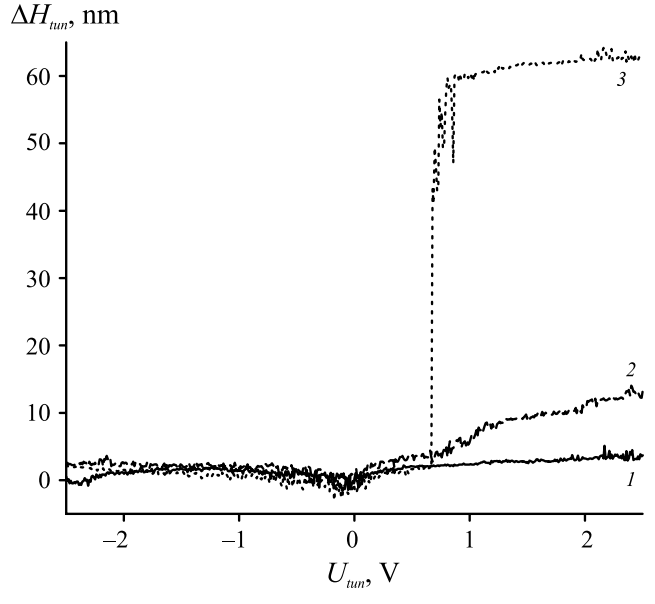

Fig. 8 Local voltage–distance spectra of ST10 sample: representative types of curves observed at various points of the sample

observation, obtained with the most resistive samples confirms the interpretation of voltage–distance anomalous behavior discussed above.

The pronounced increase of the total film resistance can result from the changes in conductivity of the crystalline solid solution SnO_2–TiO_2, and also from the increase of contribution of the poorly conducting amorphous component (both effects are assumed to be size-dependent). The specific features of fixing the tip in the gap can be the reason for the change of the nature of the image: the increase in total resistance can lead from the imaging of conductive crystalline component to the imaging of amorphous component and (or) simultaneous imaging of both components. The appearance of steps in the voltage–distance spectra agrees with the assumption about the above-mentioned change. The qualitative difference of ST20 STM images as compared to less doped films also supports this assumption; however we cannot determine the quantity of amorphous component from STM data.

Based on STM, XRD, and MS results we could propose the following model of nanostructured doped films.

The highly dispersed (on STM base) rutile phase observed in the mixed films studied in the present work may be classified as a solid solution with short-range order or as a nanocomposite containing both SnO_2 and TiO_2 nanoclusters (< 1 nm in size). Poorly ordered tin and titanium oxide nanoclusters are randomly distributed in partially hydrated amorphous tin oxide matrix. The latter are pierced by ultrafine pores, which contain H_2O molecules and Cl^- ions. The crystalline $SnCl_2$ intercalation phase has been found to be the precursor of that nanostuctured forms [2, 11]. The quantities of that rutile phase in both mixed films are approximately equal, as limited by the content of Sn(II) anionic chloro complexes in origin solution of tin and titanium chlorides. The concentration of these complexes is constant because of constant c_{HCl}.

As concerns the amorphous phase, tunneling spectroscopy evidences the remarkable increase of the resistance with TiO_2 content. For the ST20 electrode, such an increase occurs for any point of the surface (both for globules with crystalline core and completely amorphous globules). The high resistance is typical of the surface of the nanoparticles being composed of tin–titanium oxide solid solution [1, 2]. The high resistance of completely amorphous globules means that amorphous SnO_2 phase of the electrodes is also essentially enriched with TiO_2.

The remarkable increase of the amorphous mixed phase may result from the higher number of Ti (IV) hydroxyoxo complexes and higher degree of their polymerization in initial solution with concentration of $TiCl_4$ of 1 mol/l. These polymeric species, which in essence appear to be the nuclei of hydrated titanium oxide, favor the hydrolysis of $SnCl_2$. The latter process induces the formation of mixed hydrated tin and titanium oxides, which remain in amorphous state up to 450°C.

In conclusion, the existence of two types of precursors of the main components in mixed films was the reason for the different content of Sn^{2+} as observed by MS. The increase of SnO in the ST10 film in comparison to the SnO_2 film may be explained by both the dispersion of nanoparticles observed by STM and by the role of precursor of the rutile solid solution (crystalline $SnCl_2$ intercalation phase). In the course of decomposition of the latter, the amorphous SnO_2 layers containing up to 15% SnO cover the globule surface [2]. The increase in Ti component results in the higher content of tin(IV) and titanium hydrated forms [11]. Therefore we can attribute the decrease in SnO content in the ST20 film with the latter effect.

Conclusion

Doping of SnO_2 with TiO_2 results in a pronounced dispersion of the solid. This effect is induced by a 2–2.5 times decrease of nanoparticles forming the films, and also by oxide dispersion in the shorter scale. Nanoparticles consist of disordered nanostructured solid solutions (presented by SnO_2 and TiO_2 nanoclusters of nano-scale size) and amorphous phase formed by both SnO_2 and TiO_2. The portion of amorphous phase in the films under study is essentially higher than in electrode materials studied in our previous works [1, 2], and its reason is the change of hydrolysis conditions for initial solutions of salt reagents. Just this extremely high dispersity of titana, which is a component stable to reduction with lithium, can be considered as a reason of better degradation stability with simultaneous keeping high capacity values (typical of nanostructured tin oxides). Direct observation of the increase of tin dioxide dispersion with doping titania content is obtained.

The nanoheterogeneous character of the rutile phase observed in the films under study, is confirmed by XRD and MS investigations.

The decrease in particle size is assumed to be one reason for the slower degradation in the course of cycling in lithium-containing solutions (Fig. 3). Actually, the enlargement of metallic tin particles should be very slow when these particles are separated by low-conductive (and most probably amorphous) oxide with high titania content. Heterogeneity of doped films, confirmed by local tunneling spectroscopy can be considered as a possible reason of the absence of plateau. Both heterogeneity of ohmic drop and equilibrium potentials for certain redox transformations of chemically different areas can be assumed, and these two effects can hardly be differentiated at this stage.

Interpretation of electrochemical data for highly resistive films is complicated by the uncertainty of potential values, which are distorted by the ohmic drop and possible heterogeneity of potential distribution along the surface. Under these circumstances one can not exclude the selective solvent discharge at already formed metallic fragments, which gives additional contribution to the total charge.

Acknowledgements The authors are grateful to A.V. Denisov for technical support of STM and spectroscopic studies. The study is supported by RFBR, projects 03-03-32422-a, 02-03-32226-a.

References

1. Tsirlina GA, Roginskaya YuE, Postovalova GG, Vassiliev SYu (1999) Russ J Electrochemistry 35:1385
2. Postovalova GG, Roginskaya YuE, Zavyalov SA, Galyamov BSh, Klimenko NL (2000) Neorganicheskie materialy (in russian) 36:452
3. Courtney IA, Dahl JR (1997) J Electrochem Soc 144:2045
4. Courtney IA, Dahl JR (1997) J Electrochem Soc 144:2943
5. Zhu J, Lu Zh, Aruna ST, Aurbach D, Gedanken A (2000) Chem Matter 12:2557
6. Goward GR, Leroux F, Power WP, Ouvrard G, Dmovski W, Egami T, Nazar LF (1999) Electrochem Solid-State Lett 2:367
7. Idota Y, Matsufuji A, Maekawa Y, Miyasaki T (1997) Science 276:1395
8. Kulova TL, Skundin AM, Roginskaya YuE, Chibirova FKh (2004) Russ J Electrochem 40:484
9. Kulova TL, Roginskaya YuE, Skundin AM (2005) Russ J Electrochem 41:69
10. Roginskaya YuE, Morozova OV (1995) Electrochimica Acta 40:817
11. Postovalova GG, Morozova OV, Galyamov BSh, Lubnin EN, Prutchenko SG, Kozlova NV, Roginskaya YuE (1998) Russi J Inorg Chem 43:36
12. Einaga H (1979) J Chem Soc, Dalton Trans 12:1917
13. Bragina MI, Bobyrenko YuYa (1972) Russ Jo Inorg Chem 17:417
14. Zhurov VV, Ivanov SA (1993) Crystallogr Rep 42:202
15. Vassiliev SYu, Denisov AV (2000) Zhurnal tehnicheskoy fiziki (in russian) 70:100
16. Iveronova VI, Revkevich GP (1972) The theory of X-ray scattering Ed by MSU, p 124–125
17. Vassiliev SYu, Pron'kin SN, Tsirlina GA, Petrii OA (2001) Russ J Electrochem 37:523
18. Cox PA, Egdell RG, Harding C, Patterson WR, Tavener PJ (1982) Surf Sci 123:179
19. Hollamby PC, Aldridge PS, Moretti C, Egdell RG (1993) Surf Sci 280:393